

# Analysis of Water Transport in Proton Exchange Membranes Using a Phenomenological Model

P. C. Sui

Ned Djilali<sup>1</sup>

e-mail: ndjilali@uvic.ca

Institute for Integrated Energy Systems,  
Department of Mechanical Engineering,  
University of Victoria, Victoria, B.C., Canada

*An investigation of water transport across the membrane of a proton exchange membrane fuel cell is performed to gain further insight into water management issues and the overall behavior of a representative phenomenological model. The model accounts for water transport via electro-osmotic drag and diffusion and is solved using a finite volume method for a one-dimensional isothermal system. Transport properties including the water drag and diffusion coefficients and membrane ionic conductivity are expressed as functions of water content and temperature. An analytical solution based on a generalized form of the transport properties is also derived and used to validate the numerical solutions. The effects of property variations on the water flux across the membrane and on the overall membrane protonic conductivity are analyzed. The balance between transport via electro-osmotic drag and diffusion depends not only on operating conditions, such as current density and relative humidity at the membrane boundaries, but also on design parameters, such as membrane thickness and membrane material. Computed water fluxes for different humidity boundary conditions indicate that for a thick membrane (e.g., Nafion 117), electro-osmotic drag dominates the transport over a wide range of operating conditions, whereas for a thin membrane (e.g., Nafion 112), diffusion of water becomes equally important under certain humidification conditions and current densities. Implications for the resolution of membrane transport in CFD-based models of proton exchange membrane fuel cells are also discussed. [DOI: 10.1115/1.1895945]*

## Introduction

Water management is one of the critical operation issues in proton exchange membrane fuel cells (PEMFC). Spatially varying concentrations of water in both vapor and liquid form are expected throughout the cell because of varying rates of production and transport. Water emanates from two sources: the product water from the oxygen-reduction reaction in the cathode catalyst layer and the humidification water carried by the inlet streams or injected into the fuel cell. Several transport mechanisms in the cell affect water distribution. In the membrane, primary transport is through (i) electro-osmotic drag associated with the protonic current in the electrolyte, which results in water transport from anode to cathode; and (ii) diffusion associated with water-content gradients in the membrane. One of the main difficulties in managing water in a PEMFC is the conflicting requirements of the membrane and of the catalyst-gas diffusion layer. On the cathode side, excessive liquid water may block or flood the pores of the catalyst layer, the gas diffusion layer or even the gas channel, thereby inhibiting or even completely blocking oxygen mass transfer. On the anode side, as water is dragged toward the cathode via electro-osmotic transport, dehumidification of the membrane may occur, resulting in deterioration of protonic conductivity. In the extreme case of complete drying, local burnout of the membrane can result. Devising better water management is therefore a key issue in PEMFC design, and this requires improved understanding of the parameters affecting water transport in the membrane.

Polymer membranes commonly used in PEMFCs, such as Nafion, are, in general, impermeable to most gases except water; thus, transfer of water across the membrane can be considered as the only mass transfer that takes place between the anode and cathode. It is this mass transfer, in addition to heat transfer, that

makes analysis of the transport phenomena in a PEMFC complicated. Water transfer across the membrane not only changes the mass concentration distribution of gas species in the fuel cell but also affects heat transfer in the entire cell because the membrane conductivity is a function of water content in the membrane. The ohmic losses prescribed by water distribution, in turn, affect electric potential distribution in the cell as well as local consumption rates of oxygen and hydrogen. Because of these couplings, understanding of water transfer across the membrane is also required for devising effective heat management of PEMFCs.

The topic of water transport in polymer electrolyte membranes has been the subject of numerous investigations, either focused solely on the membrane or as part of fuel-cell models and simulations. Membrane models can be categorized in terms of mathematical formulation, i.e., those written in the form of a flux equation and those cast in the form of conservation equations. In the former case, the membrane is considered as a single domain, transport is taken to be essentially one-dimensional (1D), and water fluxes are obtained on the domain boundaries. Models in this category are further divided into two groups [1]: (i) hydraulic models based on the Schlögl equation, and (ii) diffusion models based on a phenomenological equation derived using Onsager's reciprocal theory. Examples of hydraulic models include Bernardi and Verbrugge [2], Gurau et al. [3], Eikerling et al. [4], Singh et al. [5], and Berning and Djilali [6]. In general, phenomenological models describe the flux as the balance arising from several driving forces, e.g., electro-osmotic drag, water diffusion, and pressure difference. Diffusion models appear to be more popular [7–13]. We note that for the flux equation based on the diffusion model, approximate solutions are often used in simulations because of the complexity of property variations of the membrane.

In fuel-cell models implemented using computational fluid dynamics (CFD) techniques, including water transport into the conservation equations, has the advantage of allowing the use of a single continuous domain to solve the problem. Um et al. [14] model the drag as a body-force term in the momentum equation and water diffusion in the species equation. The electro-osmotic

<sup>1</sup>Corresponding author.

Paper presented at the 2004 2nd International Conference on Fuel Cell Science, Engineering and Technology. Manuscript received October 4, 2004; revision received January 28, 2005. Review conducted by: A. Hernandez.

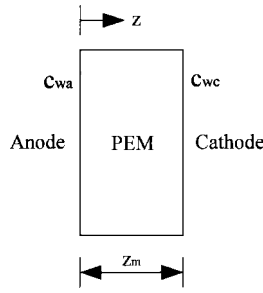


Fig. 1 Computational domain and BC

drag is accounted for in the velocity associated with the convective term in the species equation. In subsequent work, Um and Wang [15] included the drag term in the water species equation. Mazumder and Cole [16] incorporate water transport into their generalized water saturation equation and solve it as a scalar equation along with other conservation equations. Li et al. [17] also solve the water transport as a scalar equation, but their model essentially follows the phenomenological approach with a drag term and a diffusion term.

The microscopic mechanisms of water transport in polymer electrolyte membranes and their macroscopic representation are the subject of ongoing debate. In the present paper we adopt the phenomenological approach to establish a framework for CFD simulations because of its mathematical simplicity and the availability of experimental data for the macroscopic transport properties required in such a model. Although phenomenological models have been proposed for some time, a systematic analysis and assessment on such models, which is particularly important for CFD implementation, has not been performed. The objectives of the present study are to perform such an analysis and to investigate the implications for multidimensional CFD-based implementation.

### Model Equation and Numerical Solution

The generalized transport equation for water based on the phenomenological model can be written as

$$J = \frac{n_d}{F}i - \frac{\rho_m}{M_w}D_w\nabla c_w - \frac{K}{\mu}\nabla p \quad (1)$$

The variable  $c_w$  represents the number of water molecules per sulfonic acid group. The Schlögl equation used in hydraulic models can be considered a special case of Eq. (1) when the diffusion term vanishes under saturated conditions on both sides of the membrane. The permeability of water in the membrane is, in general, much smaller than the drag and diffusion terms. Neglecting the pressure term and rewriting Eq. (1) in conservation form, we have

$$\nabla J = \frac{i}{F}\nabla n_d - \frac{\rho_m}{M_w}\nabla(D_w\nabla c_w) = 0 \quad (2)$$

For a 1D configuration, Eq. (2) can be solved if the current density is known, and if either (a) the water content and flux are prescribed at each boundary or (b) the water content is known and prescribed at both boundaries. Springer et al. solved the problem with condition (a). For CFD simulations, the water flux is not usually known a priori, therefore, in the present study Eq. (2) is solved with Dirichlet conditions on the membrane surface (cf. Fig. 1)

$$c_w = c_{w,a} \quad \text{at} \quad z = 0 \quad (3)$$

and

$$c_w = c_{w,c} \quad \text{at} \quad z = z_m \quad (4)$$

The transport properties of the membrane are primarily functions of water content and temperature. A uniform temperature is as-

sumed in the calculation. We note that the solution of Eq. (2) is bounded by the boundary conditions, i.e., the maximum and minimum must appear on the boundaries. This can be proven first by assuming there exists a maximum within the membrane, and the gradient of water content at this point is then zero. From Eq. (2) we have

$$\nabla c_w = \frac{J - \frac{n_d}{F}i}{\frac{\rho_m}{M_w}D_w} = 0 \quad (5)$$

which implies

$$J = \frac{n_d}{F}i \quad (6)$$

Since there is only one flux value for the membrane and Eq. (6) applies to both boundary values, this leads to

$$c_{w,a} = c_{w,c} \quad (7)$$

which negates the assumption that there exists a maximum within the membrane. When a solution is obtained using the given boundary conditions in a fuel-cell problem, the flux required by the membrane part may not be available from the region outside of the membrane because of mass-transfer limitations from the sources near the membrane; for instance, for a dry anode when water in the gas channel is less than the predicted flux in the membrane, or for a nearly flooded cathode when further water removal from the membrane to the cathode is not possible. Under such conditions, the solution approach should change back to the aforementioned condition (a), i.e., use of a prescribed value and the limiting flux. In the present study, such limit case conditions are not considered.

The discretized form of Eq. (2) is solved numerically using the classical tridiagonal matrix algorithm (TDMA). The properties reported by Springer et al. [7] are used in the baseline calculations. Only partially saturated boundary conditions are considered in order to avoid the so-called Schröder paradox, i.e., the jump in the number of water molecules between liquid water and vapor equilibrated states. The water content in the electrolyte phase is related to water activity via

$$c_w = 0.043 + 17.81a - 39.85a^2 + 36a^3 \quad (8)$$

For the vapor phase on the membrane surface the water activity is equal to the relative humidity. The drag coefficient is expressed as a linear function of water content

$$n_d = \frac{2.5}{22}c_w \quad (9)$$

We note that Zawodzinski et al. [18] reported a unity drag coefficient when Nafion is equilibrated with water vapor. The diffusion coefficient given by Springer et al. [7] is written as

$$D_w = \frac{c_w}{(1 + s \cdot c_w)^2} \frac{da}{dc_w} D' \quad (10)$$

where  $s=0.126$  is the swelling factor and  $D'$  is fitted piecewise as

$$D' = 0.25c_w, \quad 0 < c_w \leq 2$$

$$D' = 0.5 + 0.8125(c_w - 2), \quad 2 < c_w \leq 6$$

$$D' = 3.75 + 0.267(c_w - 6), \quad 6 < c_w \quad (11)$$

Figure 2 shows a comparison of the water diffusion coefficient of Springer et al. [7] versus correlations reported by other researchers. There are two types of curves: those with a maximum value near  $c_w=3$  (ca. relative humidity (RH)=0.5 in Fig. 3) and those linearly proportional to  $c_w$ . The curve by Motupally et al. [19] is, in fact, derived from Springer et al. [7] with a quadratic polynomial fit for  $D'$ . We note that the diffusion coefficient is sensitive to

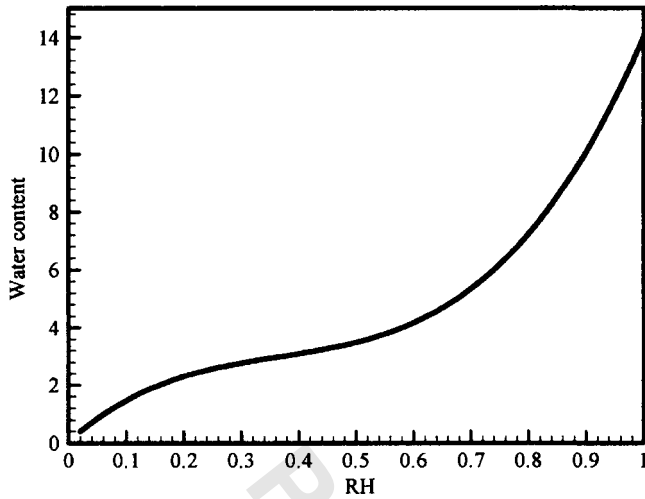


Fig. 2 Diffusion coefficients used in calculation

temperature. Figure 3 shows that the peak value using the correlation of Springer et al. at 353 K is about a factor of three higher than at 303 K. The protonic conductivity of the electrolyte is given by

$$\sigma = (0.005139c_w - 0.00326)\exp\left[1268\left(\frac{1}{303} - \frac{1}{T}\right)\right] \quad (12)$$

(cf. Fig. 4), which is higher than that reported by Sone et al. [20]. The resistance of the membrane is calculated by

$$R = \int_0^{z_m} \frac{1}{\sigma} dz \quad (13)$$

Membrane density  $\rho_m = 2000 \text{ kg/m}^3$  and equivalent weight  $M_w = 1.1 \text{ kg/mol}$  are used in the calculation. Temperature is set to at 353 K unless otherwise specified.

An analytical solution for the generalized water transport equation (1) without the pressure-gradient term is also derived in the present study for validation of the numerical solution of (2). Assuming a general form for the water flux across the membrane,

$$J = f(c_w, T) + g(c_w, T)\nabla c_w \quad (14)$$

Rearranging and integrating (14) and using the fact, as shown earlier, that water content varies monotonically across the mem-

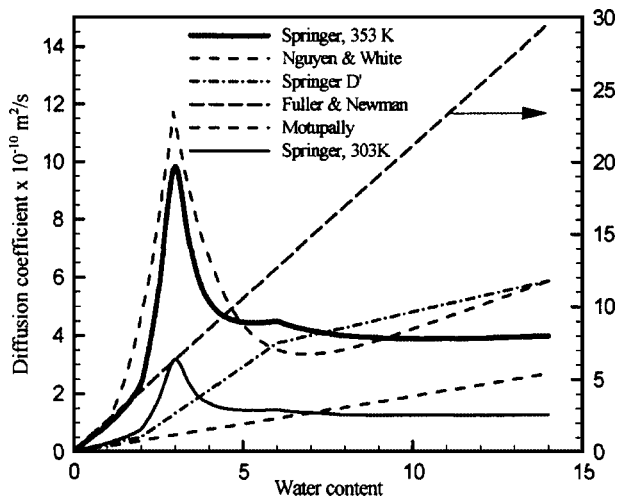


Fig. 3 Sorption isotherm of Nafion

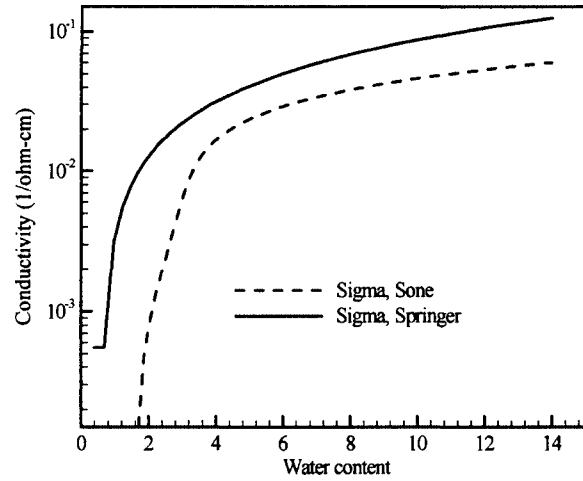


Fig. 4 Protonic conductivity of Nafion by Springer et al. [7] and Sone et al. [20]

brane, we obtain an analytical solution for the flux in an implicit form

$$\int_{c_{wa}}^{c_{wc}} \frac{g}{J-f} dc_w = \int_0^{z_m} dz = z_m \quad (15)$$

The solution for  $J$  is the root satisfying a function defined by

$$\Gamma \equiv \int_{c_{wa}}^{c_{wc}} \frac{g}{J-f} dc_w - z_m = 0 \quad (16)$$

Root-finding methods, such as the Newton-Raphson method, can be used to solve for  $J$  in (16). The derivative with respect to flux  $J$  in (16), which is required when the Newton-Raphson method is used, can be expressed as

$$\Gamma' = \int_{c_{wa}}^{c_{wc}} \frac{d}{dJ} \left( \frac{g}{J-f} \right) dc_w = - \int_{c_{wa}}^{c_{wc}} \frac{g}{(J-f)^2} dc_w \quad (17)$$

Once the flux is calculated, the water-content profile in the membrane can be calculated from

$$\int_{c_{wa}}^{c_w} \frac{g}{J-f} dc_w = z \quad (18)$$

The membrane resistance can then be calculated by substituting the differential form of (18) into (13) for  $dz$ , i.e.,

$$R = \int_0^{z_m} \frac{1}{\sigma} dz = \int_{c_{wa}}^{c_{wc}} \frac{g}{(J-f)\sigma} dc_w \quad (19)$$

A numerical integration routine is required for Eqs. (17)–(19). One of the advantages of the analytical solution over the discretized solution is that no grid is required, and grid resolution plays no role in the solution accuracy. A similar analytical approach was recently reported by De Francesco et al. [21], which included the flux term due to pressure gradient and expressed the transport equation in a dimensionless form.

## Results and Discussion

We first validate the finite-volume solution by comparing the numerical and analytic water profiles in Fig. 5, using the properties given in Springer et al. [7]. The numerical results using 200 uniform grids across the membrane are found to be in very close agreement with the analytical solution. Figure 6 shows the predicted water-content profiles using several different expressions for the water diffusion coefficient. The boundary conditions are chosen to include the peak of  $D_w$  for the Springer-type diffusion

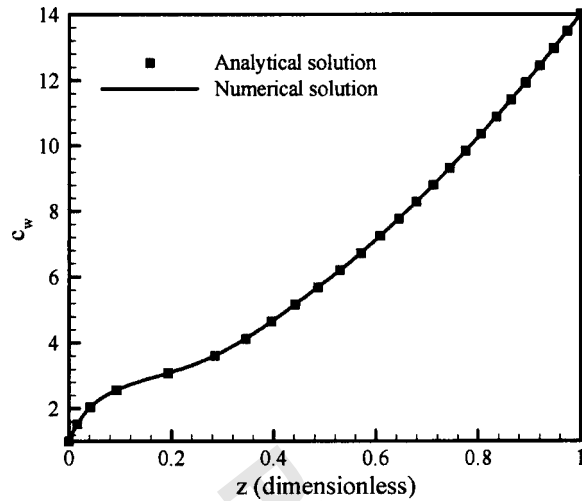


Fig. 5 Comparison of analytical solution and numerical solution

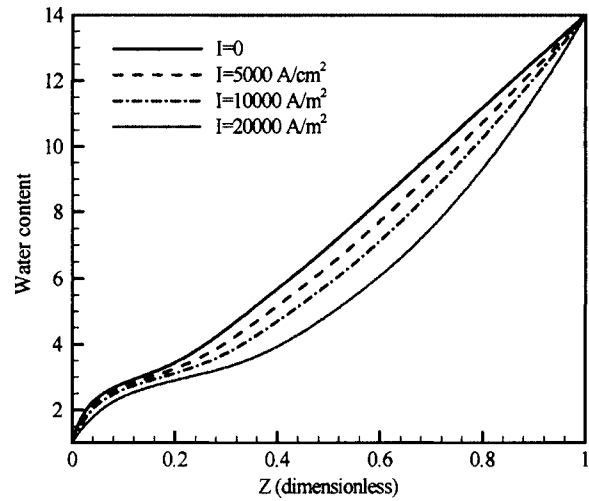


Fig. 7 Water-content profiles at different current density for membrane thickness 50  $\mu\text{m}$

coefficient in the solution range. In this example, the water content is set at an extremely low value on one side of the membrane in order to demonstrate the impact of diffusion-coefficient correlation on the numerical predictions. Table 1 lists the predicted flux and IR (ohmic) loss of the membrane. The water profiles calculated using the Springer-type diffusion coefficient are similar in shape, with a minimum gradient near the water content corresponding to maximum  $D_w$  values. The flux and IR loss calculated using similar diffusion coefficient curves (cf. Motupally [19] versus present study), still show noticeable differences. It is interesting to note that for the Springer-303 K case and the Nguyen-

White case, even though the diffusion coefficients are in the same range, the calculated fluxes and IR losses are quite different. This is because at low  $c_w$ , diffusion dominates water transport in Springer's model, whereas drag is dominant in Nguyen and White's model. As a result, the diffusion-dominated case yields a negative flux (from cathode to anode) and the drag-dominated case yields a positive flux. The profile obtained using the Fuller-Newman curve (note different scale in Fig. 3) is another example of a diffusion-dominated case. From Table 1, one can see that when  $c_{w,c} > c_{w,a}$ , higher diffusion produces a higher flux from cathode to anode and lower IR losses. For the Springer case at 303 K, the IR loss is higher than that at 353 K by a factor of 2.5. This increase is higher than that due to the temperature factor alone, (ca. 1.8 from Eq. (12)). The additional increase is mainly due to the lower  $c_w$  profile associated with the lower diffusion coefficient for the 303 K case.

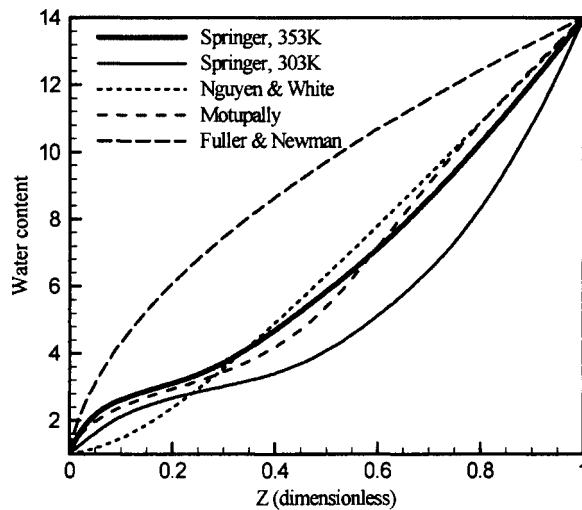


Fig. 6 Predicted water-content profiles using different diffusion-coefficient expressions, membrane thickness 50  $\mu\text{m}$  at  $I=10,000 \text{ A/m}^2$

Table 1 Summary of predicted flux and IR loss using diffusion coefficient curves in Fig. 6

	$J$ (mol/m <sup>2</sup> s)	$R$ ( $\Omega \text{ m}^2$ )
Springer et al. [7], 353 K	-0.125	0.147
Springer et al. [7], 303 K	-0.0275	0.364
Nguyen and White [9]	0.100	0.227
Motupally et al. [19]	-0.153	0.158
Fuller and Newman [8]	-0.641	0.871

Figure 7 shows the water-content profiles calculated over a range of current densities. With increasing current density, the relative strength of the drag term over the diffusion term in Eq. (2) increases. For the case of  $c_{w,c} > c_{w,a}$ , as current density increases, the  $c_w$  profile shifts toward the cathode side because of the drag. As a result, the membrane resistance increases (cf. Fig. 8). As the

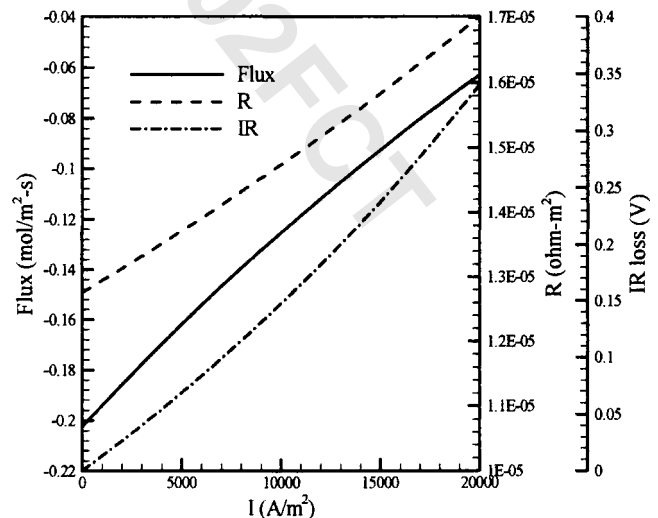
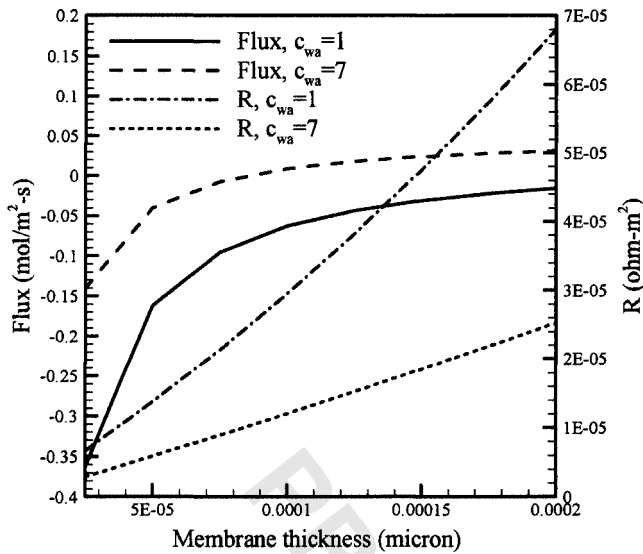


Fig. 8 Flux, membrane resistance, and IR loss at different current density for  $z_m=50 \mu\text{m}$ ,  $c_{w,a}=1$  and  $c_{w,c}=14$



**Fig. 9 Flux and membrane resistance at different membrane thickness**

drag term becomes stronger, water transport from cathode to anode decreases, i.e., the water flux becomes less negative. Even with the nonlinear profiles in Fig. 7, the IR loss, and likely the cell voltage on the polarization curve too, appears to vary quasi-linearly with current density. Figure 9 shows predicted flux and membrane resistance versus membrane thickness for two different water contents  $c_{w,a}$  at the anode. As shown in Eq. (2), increasing membrane thickness reduces the strength of diffusion and this has similar effects when  $c_{w,a}$  is increased for a fixed  $c_{w,c}$ . For the case  $c_{w,a}=1$ , over the membrane-thickness range tested, the water flux is all negative, whereas for the case of  $c_{w,a}=7$ , the drag term begins to balance the diffusion term at ca.  $85 \mu\text{m}$  and the water flux becomes positive from this point on.

Figure 10 compares water-content profiles for opposite boundary conditions for two membrane thicknesses. Unlike the case discussed thus far for  $c_{w,c} > c_{w,a}$  and in which drag opposes diffusion (denoted as drag  $\times$  diffusion), when  $c_{w,a} > c_{w,c}$ , the diffusive transport is in the same direction as the drag term (denoted as drag//diffusion). The effect of the direction of drag with respect to diffusion becomes clear if we flip curve A (drag//diffusion) in Fig.

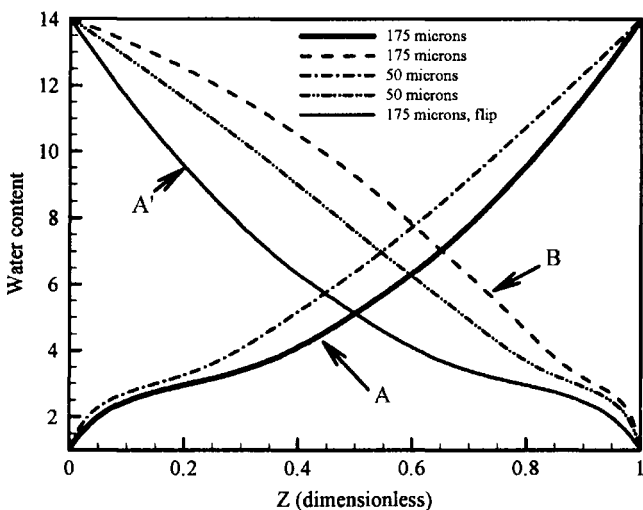


**Fig. 10 Water-content profiles at different boundary conditions,  $I=5000 \text{ A/m}^2$**

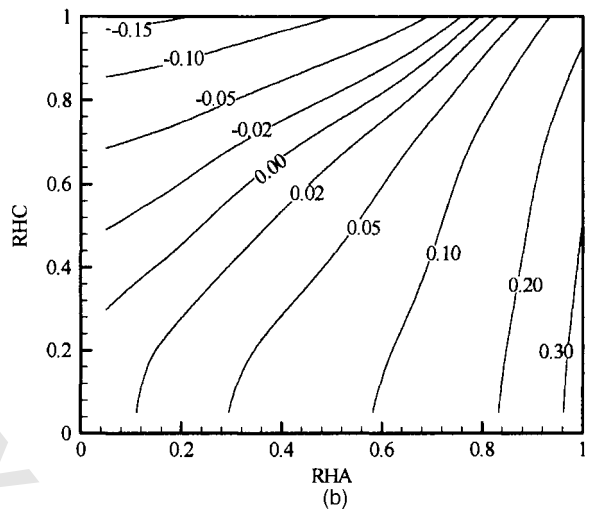
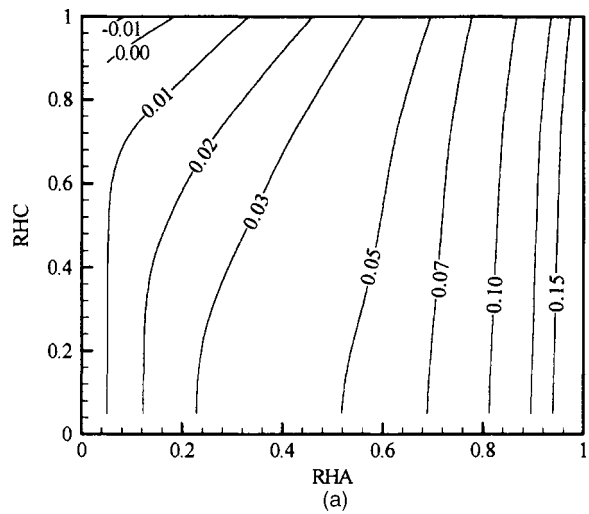


**Fig. 11 Flux predictions ( $\text{mol/m}^2\cdot\text{s}$ ) for different relative-humidity conditions on both sides of membrane for  $I=10,000 \text{ A/m}^2$  and membrane thickness (a)  $175 \mu\text{m}$  and (b)  $50 \mu\text{m}$**

10 and compare this curve (A') to profile B (drag  $\times$  diffusion). For drag//diffusion, the water content profile is always higher than that of drag  $\times$  diffusion. The membrane resistance is therefore lower for the drag//diffusion case. For the thinner membrane (Nafion 112) in Fig. 10, the effect of drag and diffusion direction is similar but less pronounced because diffusion is inherently stronger than drag for the thin membrane.

The point where the water flux changes direction is of interest for design and operation; it is clear from the discussion that this point depends on a number of factors. Because of the nonlinear properties, simple dimensionless parameters to determine the transition point are not readily obtainable, but the data can be conveniently presented in the form of two-dimensional (2D) maps. Figures 11(a) and 11(b) show the flux prediction map for a current density of  $10,000 \text{ A/m}^2$  subject to a wide range of humidity boundary conditions for Nafion 117 and 112, respectively. For Nafion 117, the flux is positive (anode to cathode) for most conditions, except for a small portion on the map corresponding to a sufficiently high water content difference. This highlights the need for humidification when using thick membranes, such as Nafion 117. For a thin membrane, such as Nafion 112, a good portion of the map exhibits a negative water flux. Since the humidity on the membrane surface is mainly dependent on the humidity in the gas channel, this suggests that if the flow-field plate is designed care-

fully to take advantage of the characteristics shown on this flux map, effective water management could, in principle, be achieved with little humidification.

Because the water transport problem involves complex and rapid property variations that have the potential of inducing numerical instabilities, some CFD-based models for PEMFC rely on an approximate solution to account for the water flux on both sides of the membrane. A common approximation for the flux is given by

$$J_w = n_{\text{drag}}(\bar{c}_w) \cdot \frac{\bar{t}^+}{F} - D_w(\bar{c}_w) \cdot \frac{c_{w,c} - c_{w,a}}{z_m} \quad (20)$$

where the average water content used to evaluate membrane properties is

$$\bar{c}_w = \frac{c_{w,a} + c_{w,c}}{2} \quad (21)$$

The drag term in Eq. (20) is a reasonable approximation for a linear or constant drag coefficient. The approximate diffusion term, however, can be problematic near water content where large variations in the diffusion coefficient occur or for cases with a large difference in the humidification between anode and cathode. To assess the error in the solution based on the approximate form, we define a relative error based on the maximum flux, defined as the sum of the absolute value of the two terms in the flux equation

$$\varepsilon \equiv \frac{J_{\text{ref}} - J_{\text{approx}}}{J_{\text{max}}} = \frac{J_{\text{ref}} - J_{\text{approx}}}{J_{\text{drag}} + |J_{\text{diff}}|} \quad (22)$$

where

$$J_{\text{drag}} = \frac{n_d}{F} i \quad (23)$$

$$J_{\text{diff}} = -\frac{\rho}{M_w} D_w \nabla c_w \quad (24)$$

$J_{\text{ref}}$  is the “exact” numerical solution, and  $J_{\text{approx}}$  is the flux evaluated using Eq. (20). Figures 12(a) and 12(b) show the relative error defined as Eq. (22) for Nafion 117 and Nafion 112, respectively. Near the diagonal line (equal humidity conditions at anode and cathode) the error is small. The error becomes increasingly higher as we move away from the equal humidity conditions, and the error map exhibits two local maxima in the vicinity of RHA = 0.7 for low RHC, and RHC = 0.7 for low RHA. Since the error in the drag term is smaller, the relative error stems primarily from the diffusion term. From Figs. 2 and 3 one can see the RH for maximum  $D_w$  is roughly  $\text{RH} \approx 0.5$ . Because the diffusion term depends on the product of  $D_w$  and the gradient of  $c_w$ , a local error maximum is attained at  $\text{RH} = 0.7$ . A similar error-map pattern is observed for Nafion 112 in Fig. 12(b), but on average the error is larger for the Nafion 112 case because of the higher relative strength of diffusion over drag. For Nafion 117, most of the flux on the map is positive, i.e., the flux is underestimated by the approximate solution. For Nafion 112, in addition to the error in magnitude of flux, there are also conditions where the approximate solution predicts flux in the opposite direction with respect to the actual flux direction.

### Conclusions

In this paper we reported on an analysis of water transport and management of PEMFCs based on the numerical solution of a phenomenological transport equation accounting for electro-osmotic drag and diffusion. An analytical solution based on a generalized form of the transport properties is also derived and used to validate the numerical model. The solutions of the transport equation indicate that water transport through the membrane is determined by the relative strength of the drag and the diffusion term, which is affected by parameters, such as membrane thick-

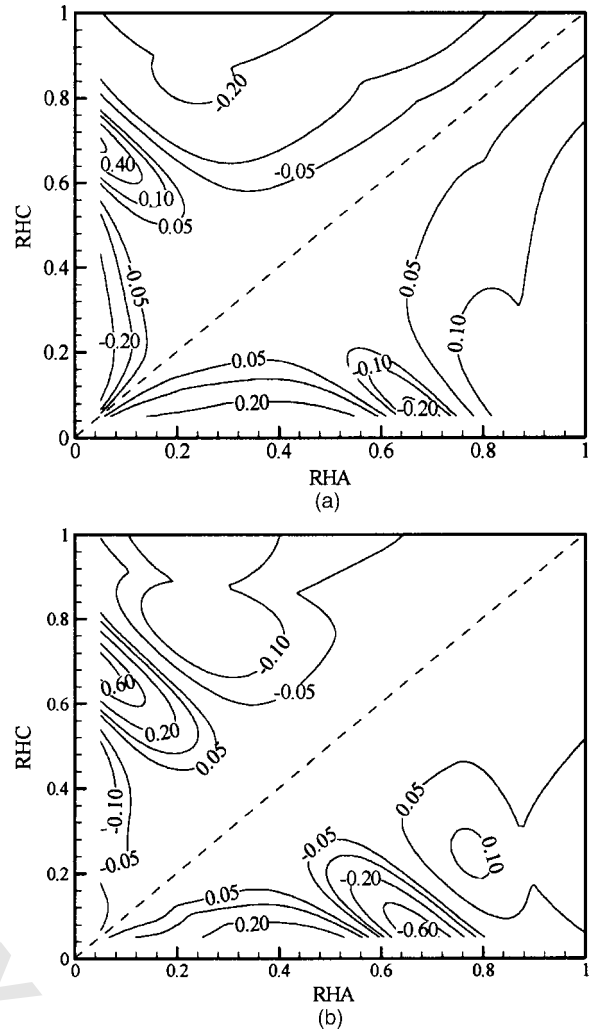


Fig. 12 Relative error of approximated solutions for  $c_{w,a}=1$ ,  $c_{w,c}=14$ ,  $i=10,000 \text{ A/m}^2$  for membrane thickness of (a)  $175 \mu\text{m}$  (Nafion 117) and (b)  $50 \mu\text{m}$  (Nafion 112)

ness, as well as operating conditions, such as relative humidity (RH) at the membrane boundaries and current density.

For a thick membrane, such as Nafion 117, the flux map shows that under most RH conditions the water flux is positive, indicating the need for humidification on the anode when operating the fuel cell. For a thin membrane, such as Nafion 112, negative water flux may occur under certain conditions. Since the protonic conductivity of the membrane is a function of water content, the impact on membrane resistance because of water transport is significant. When the water content of the membrane on the anode side is lower than that on the cathode side, the overall membrane resistance increases with increasing current density. On the other hand, when the conditions are reversed such that the humidification is higher on the anode side and both drag and diffusion are in the same direction, the overall membrane resistance decreases with increasing current density.

The present study is part of a program aimed at developing comprehensive CFD simulation tools for PEMFCs. The error analysis presented in this paper shows that approximate formulations typically used in CFD models result in significant errors in estimating water fluxes in the presence of either large gradients of water content or significant variation in the diffusion coefficient. The analytical solution presented in this paper can be implemented into a CFD code to replace discrete solutions and to ac-

count more accurately for water transport across the membrane. The analytical solution can also be incorporated in simplified, along-the-channel types of fuel-cell models.

### Acknowledgments

This work was performed with the support of the MITACS Network of Centres of Excellence and Ballard Power Systems.

### Nomenclature

- $a$  = water activity, dimensionless  
 $c_w$  = water content, dimensionless  
 $D'$  = diffusion coefficient,  $m^2/s$   
 $D_w$  = water diffusion coefficient,  $mol/m^2 s$   
 $F$  = Faraday constant, 96,487 C  
 $f$  = generalized water drag coefficient  
 $g$  = generalized water diffusion coefficient  
 $i$  = current density,  $A/m^2$   
 $J$  = water flux,  $mol/m^2 s$   
 $M_w$  = equivalent weight of a dry membrane,  $kg/mol$   
 $n_d$  = electro-osmotic drag coefficient, dimensionless  
 $T$  = temperature, K  
 $P$  = pressure, Pa  
 $R$  = membrane resistance,  $\Omega$   
 $RH$  = relative humidity, dimensionless  
 $s$  = swelling factor, dimensionless  
 $z$  = membrane coordinate, m  
 $z_m$  = membrane thickness, m

### Greek

- $\rho_m$  = density of a dry membrane,  $kg/m^3$   
 $\sigma$  = ionic conductivity, S  
 $\Gamma$  = function defined in Eq. (16)

### Subscript

- $a$  = anode side of the membrane  
 $c$  = cathode side of the membrane

### References

- [1] Weber, A. Z., and Newman, J., 2003, "Transport in Polymer-Electrolyte Membranes—I. Physical Model," *J. Electrochem. Soc.* **150**(7), pp. A1008–A1015.
- [2] Bernardi, D. M., and Verbrugge, M. W., 1992, "A Mathematical-Model of the Solid-Polymer-Electrolyte Fuel-Cell," *J. Electrochem. Soc.* **139**(9), pp. 2477–2491.
- [3] Gurau, V., Liu, H. T., and Kakac, S., 1998, "Two-Dimensional Model for Proton Exchange Membrane Fuel Cells," *AIChE J.* **44**(11), pp. 2410–2422.
- [4] Eikerling, M. Kharkats, M. Y. I., Kornyshev, A. A., and Volkovich, Y. M., 1998, "Phenomenological Theory of Electro-Osmotic Effect and Water Management in Polymer Electrolyte Proton-Conducting Membranes," *J. Electrochem. Soc.* **145**(8), pp. 2684–2699.
- [5] Singh, D., Lu, D. M., and Djilali, N., 1999, "A Two-Dimensional Analysis of Mass Transport in Proton Exchange Membrane Fuel Cells," *Int. J. Eng. Sci.* **37**, pp. 431–452.
- [6] Berning, T. and Djilali, N., 2003, "Three-Dimensional Computational Analysis of Transport Phenomena in a PEM Fuel Cell - A Parametric Study," *J. Power Sources* **124**(2), pp. 440–452.
- [7] Springer, T. E., Zawodzinski, T. A., and Gottesfeld, S., 1991, "Polymer Electrolyte Fuel-Cell Model," *J. Electrochem. Soc.* **138**(8), pp. 2334–2342.
- [8] Fuller, T. F. and Newman, J., 1993, "Water and Thermal Management in Solid-Polymer-Electrolyte Fuel-Cells," *J. Electrochem. Soc.* **140**(5), pp. 1218–1225.
- [9] Nguyen, T. V. and White, R. E., 1993, "A Water and Heat Management Model for Proton-Exchange-Membrane Fuel-Cells," *J. Electrochem. Soc.* **140**(8), pp. 2178–2186.
- [10] Janssen, G. J. M., 2001, "A Phenomenological Model of Water Transport in a Proton Exchange Membrane Fuel Cell," *J. Electrochem. Soc.* **148**(12), pp. A1313–1323.
- [11] Dutta, S., Shimpalee S. S., and Van Zee, J. W., 2001, "Numerical Prediction of Mass-Exchange Between Cathode and Anode Channels in a PEM Fuel Cell," *Int. J. Heat Mass Transfer* **44**(11), pp. 2029–2042.
- [12] Siegel, N. P., Ellis, M. W., Nelson, D. J., and von Spakovsky, M. R., 2003, "Single Domain PEMFC Model Based on Agglomerate Catalyst Geometry," *J. Power Sources* **115**(1), pp. 81–89.
- [13] Kulikovskiy, A. A., 2003, "Quasi-3D Modeling of Water Transport in Polymer Electrolyte Fuel Cells," *J. Electrochem. Soc.* **150**(11), pp. A1432–A1439.
- [14] Um, S., Wang, C. Y., and Chen, C. S., 2000, "Computational Fluid Dynamics Modeling of Proton Exchange Membrane Fuel Cells," *J. Electrochem. Soc.* **147**(12), pp. 4485–4493.
- [15] Um, S. and Wang, C. Y., 2004, "Three-Dimensional Analysis of Transport and Electrochemical Reaction in Polymer Electrolyte Fuel Cells," *J. Power Sources* **125**, pp. 40–51.
- [16] Mazumder, S. and Cole, J. V., 2003, "Rigorous 3-D Mathematical Modeling of PEM Fuel Cells - II. Model Predictions With Liquid Water Transport," *J. Electrochem. Soc.* **150**(11), pp. A1510–A1517.
- [17] Li, S. P., Becker, U., Makarov, B., and Orsino, S., 2003, "CFD Modeling of PEMFC—Theory and Case Studies," *Fuel Cell Seminars*, Miami Beach, FL.
- [18] Zawodzinski, T. A., Springer, T. E., Davey, J., Jestel, R., Lopez, C., Valerio, J., and Gottesfeld, S., 1993, "A Comparative-Study of Water-Uptake by and Transport Through Ionomeric Fuel-Cell Membranes," *J. Electrochem. Soc.* **140**(7), pp. 1981–1985.
- [19] Motupally, ■., et al.
- [20] Sone, Y., Ekdunge, P., and Simonsson, D., 1996, "Proton Conductivity of Nafion 117 as Measured by a Four-Electrode AC Impedance Method," *J. Electrochem. Soc.* **143**(4), pp. 1254–1259.
- [21] De Francesco, M., Arato, E., and Costa, P., 2004, "Transport Phenomena in Membranes for PEMFC Applications: An Analytical Approach to the Calculation of Membrane Resistance," *J. Power Sources* **132**, pp. 127–134.